

Design and Analysis of Quad Dumbbell Shaped Directive UWB Antenna for Microwave Tumour Detection Integrated with Meander Strip Resonators

Asheesh Gupta and Madan Lal Meena*

Department of Electronics Engineering, Rajasthan Technical University, Kota, Rajasthan, India

ABSTRACT: A novel design of a dumbbell shape quad elliptical slotted (DSQES) antenna for directive ultra-wideband (UWB) integrated with WCDMA, WLAN, and mid-band of 5G applications is presented. Initially, a circular patch is designed by inserting four elliptical slots in radiator with a rectangular slotted ground plane. To realize ultra-wide impedance bandwidth, three symmetrical stepped rectangular slots are inserted in ground below a stepped-quarter-wave-transformer feed line. The proposed antenna achieves fractional bandwidth (FBW) of 104% ($S_{11} < -10$ dB) which covers UWB frequency range of 5.4–17.3 GHz at resonant frequencies 5.8/7.4/10.3/12/15.7 GHz. Further, a ground structure is customized by loading two asymmetrical meander strip resonators (MSRs), which provides extra lower frequency bands 2.1 GHz (1.96–2.21 GHz) and 3.5 GHz (3.22–4.07 GHz) for WCDMA, WLAN, and 5G mid-band applications, respectively. Furthermore, the measured gain and half-power-beam-width (HPBW) are 1.7–6.4 dBi and 75° – 20° in 5.4–17.3 GHz UWB, respectively. The optimized dimension of proposed antenna is 30×30 mm² which is simulated on Computer Simulation Technology (CST) electromagnetic simulator using an FR-4 substrate of thickness 1.6 mm and dielectric constant 4.3. The simulated structure is computed by ADS simulator, and simulated results are validated with measured ones.

1. INTRODUCTION

In the present scenario there is always the need for directive ultra-wideband antennas which are also attuned for Bluetooth, Wi-Max, WCDMA, WLAN, and 5G applications at lower frequency. Due to the compact size and low cost, such types of antennas are easy to integrate and more versatile with modern wireless equipment [1]. Without affecting the directional UWB characteristics, the major challenges in the design of these antennas with multiband applications are impedance matching, electromagnetic interference, stable radiation characteristics, and compact size [2–6].

From the literature, most of the researchers focus on the design of directional UWB antenna with defected ground structure to achieve ultra-wideband, moderate gain, and directivity [7–10]. Meena et al. designed elliptical and circular ring having defected ground structure directional UWB antennas for microwave imaging, radar systems, C & X band applications with good directional characteristics and size 40×40 mm², but reported antennas are limited to UWB only [11–15]. Further, the design of multiband antennas was proposed with size 160×160 mm² and operating frequency in the range of 5–5.5 GHz, but applications of the proposed antennas are for lower wireless band only without covering UWB [16–20].

Further in [21–23], a circular ring having triangular and arc-shaped antenna was proposed for UWB along with WLAN and Bluetooth applications, and a rectangular strip is loaded for covering GSM band. Aravinda et al. [24] reported a dual-band antenna for GSM/UMTS/LTE with UWB, but its dimensions

are 65×30 mm² due to large size which is difficult to use in portable devices. Daghari et al. [25] and Kapoor et al. [26] presented a wideband antenna for 5G wireless applications by introducing elliptical antenna element and defected ground structure, but it has low fractional bandwidth around 50% and size constraint 92×88 mm². Furthermore, Srivastava et al. [27], and Sohi and Kaur [28] presented an O-shaped multiband antenna design and a dual-port microstrip-fed semi-circular patch antenna with Koch curve fractals, respectively. These antennas cover UWB of 5.24–10.75 GHz with Bluetooth and WLAN, but they have low fractional bandwidths of 68% and 77%, respectively. Suvarna et al. [29] and Ken and Yang [30] proposed a tri-band miniaturized antenna using fractal defected ground structure and a tri-mode hybrid antenna. However, these antennas cover C/X, Ku-band and GPS/WLAN/Wi-Max system but does not cover UWB. Further, Patel and Makwana [31] and Kumar et al. [32] presented multiband and miniaturized antennas for GPS, IRNSS, Sub-6 GHz 5G, WLAN, Wi-Max, C-band, and X-band applications, but it also does not cover UWB.

In view of the above literature, it is clear that most of researchers focused on the design of either directional UWB antenna or multiband antenna which does not cover UWB or integration of UWB with multiband wireless communication applications. It also has limitation of large antenna size and low fractional bandwidth. It is always challenging to integrate multibands due to the coupling between different elements present in patch as well as ground plane, and another limitation of a multiband antenna is its narrow bandwidth and poor impedance matching. These limitations can be overcome by introducing

* Corresponding author: Madan Lal Meena (madan.meena.ece@gmail.com).

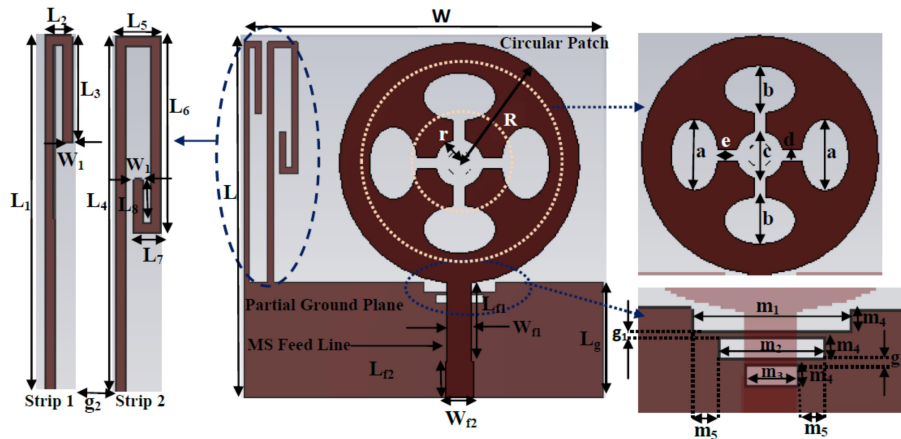


FIGURE 1. Proposed configuration of antenna with all dimensions.

slots in patch antenna and ground plane as well as integrating strip resonators in partial ground plane.

Therefore, motivation of this article is to design a directional UWB antenna integrated with multiband. In this article, a novel design of a circular radiator having a quad elliptical dumbbell shaped slot antenna is designed for directional UWB. Further, the integration of multiband can be achieved by adding two asymmetrical meander strip resonators (MSRs) of rectangular shape on the top corner of rectangle partial ground plane. The proposed design achieves 104% fractional bandwidth (FBW); gain ranges from 2.3 to 6.4 dBi; and HPBW moves between 75° and 20° in UWB of 5.4–17.30 GHz along with additional wireless bands of 1.96–2.21 GHz, 3.22–4.07 GHz for WCDMA, WLAN, and mid band of 5G applications. This structure supports UWB applications along with integration of wireless services to make this antenna more versatile. Due to highly directional characteristics it can also be used for microwave tumour detection. Further, antenna parameters such as bandwidth, gain, fractional bandwidth, half power beamwidth, and dimensions are compared with previously reported antennas [10–15, 17, 21–24, 26, 27, 29–31, 36] in available literature. The optimized dimensions is simulated, fabricated, and validated by experimental results.

The work is presented in five sections. Section 2 elaborates the proposed configuration of antenna, design method of the proposed antenna, parametric analysis, and equivalent model. In Section 3, measured results and discussions are reported. Section 4 represents antenna application and comparative analysis. Finally, conclusions are reported in Section 5.

2. PROPOSED CONFIGURATION OF ANTENNA, DESIGNING METHOD AND PARAMETRIC ANALYSIS

2.1. Proposed Configuration

The proposed structure of UWB antenna with all the dimensions is as given in Fig. 1. It is etched on a low cost FR-4 substrate having thickness $h = 1.5$ mm, relative permittivity $\epsilon_r = 4.3$, and loss tangent of 0.02. The antenna consists of a circular patch having radius R , and four equal elliptical

slots have been inserted in patch. It has a partial rectangle-shaped ground plane integrated with two asymmetrical meander strip resonators and three symmetrical rectangular stepped slots, which are inserted below 50 ohm feed line. These slots are integrated with a stepped quarter wave transformer for good impedance matching.

Three symmetrical slots are introduced in the ground plane which is equally separated to achieve UWB impedance matching. Optimized separation and width of each slot are g_1 and m_4 , respectively. Optimized length for slot-1 is m_1 , for slot-2 is m_2 , and for slot-3 is m_3 . To design an easy configuration, two asymmetrical meander strip resonators are placed on the top edge of ground plane and along the y -axis (vertically upwards). The separation between strip-1 and strip-2 is g_2 having equal height above the ground plane for both the strips. The width and length of the substrate are given by W and L , respectively. The dimensions of the proposed antenna configuration are $30 \text{ mm} \times 30 \text{ mm}$ ($1.1\lambda_o \times 1.1\lambda_o$); the lowest resonating frequency is 5.8 GHz; and free space wavelength is given by λ_o . Optimized parameters of the proposed antenna structure are given in Table 1, and subsequently the antenna is simulated on EM simulator (CST-Microwave Studio).

TABLE 1. Optimized parameters of the proposed antenna configuration.

Parameter	Value in mm	Parameter	Value in mm
$L = W$	30	Lf_1	6.6
R	10	Wf_2	2.4
$L_1 = L_4$	20	$Wf_1 = e = m_3 = r$	2
$L_2 = L_7$	1.5	$b = c = m_2$	4
$L_3 = a = m_1$	6	$d = m_5$	1
L_5	2.5	m_4	0.8
L_6	11	g_1	0.2
$L_8 = Lf_2$	3	g_2	0.5
L_g	9.6		

Design stages of the proposed antenna involve four stages as shown in Fig. 2. Antenna 1 is designed by inserting four elliptical shape slots with length of major axis $a = 6$ mm and minor axis $b = 4$ mm in a circular patch having outer radius R , inner

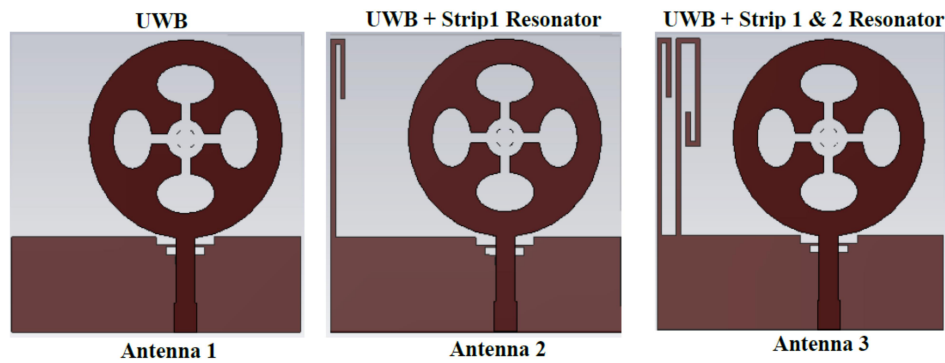


FIGURE 2. Design stages for the proposed antenna.

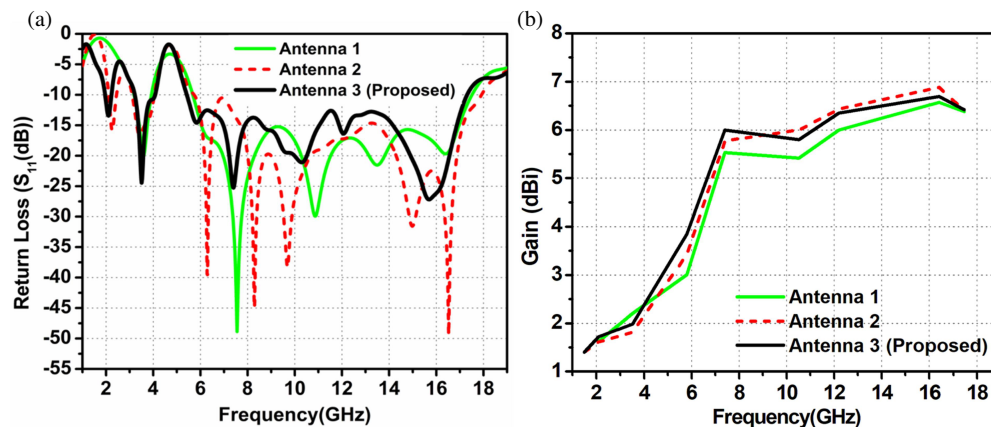


FIGURE 3. (a) Return loss vs. frequency plot for different antenna configurations (1–3). (b) Gain (dBi) vs. frequency plot for different antenna configurations (1–3).

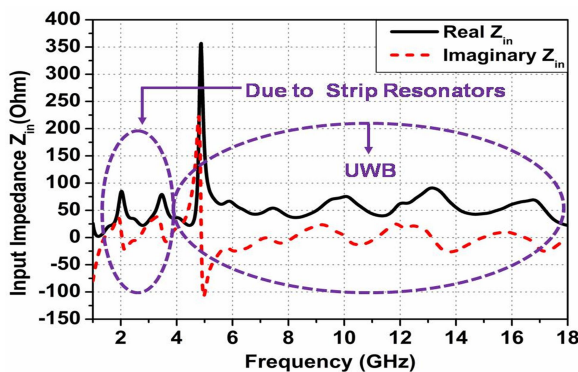


FIGURE 4. Input impedance vs. frequency plot for proposed antenna configuration.

radius r , and partial ground plane with optimized dimensions W (width) and L_g (length) without any meander strips. It is excited by a $50\ \Omega$ microstrip line, and its lowest resonant frequency is 3.6 GHz. It also covers UWB (5.7–17.5 GHz) with four resonating frequencies 7.5/10.9/13.5/16.4 GHz.

It can be seen from Fig. 3(a) that Antenna 1 offers the lowest frequency at 3.6 GHz along with UWB due to circular patch. However, in order to meet the objective to design a UWB antenna with multiband applications further, resonating strips are added to the ground plane.

More resonance at lower frequency can be excited by adding two more strips with the ground plane in which both strips are capacitive meander strip resonator. The size of strips and their positioning are adjusted in such a manner that there is no coupling between them, and desired resonance frequency is achieved at the same time. Impedance bandwidth of these strips can be tuned independently. A meander strip resonator could be added to the upper left edge of the ground plane as shown in Antenna 2 of Fig. 2. An extra resonance at a frequency of 2.25 GHz is generated with this strip-1 resonator. Further, one more folded strip-2 resonator is added at a separation of g_1 as shown in Antenna 3 of Fig. 2. It gives rise to the proposed antenna structure as shown in Fig. 2 [Antenna 3]. This proposed antenna gives resonating frequencies at 2.1 GHz, 3.5 GHz, and UWB from 5.4 to 17.3 GHz.

Plots for return loss ($|S_{11}|$ dB) and gain vs. frequency plots for different configurations of antennas (Antennas 1–3) are as shown in Figs. 3(a) and 3(b), respectively. The comparative analysis of bandwidth, fractional bandwidth, and gain variation is given in Table 2.

The resonant modes of antenna are investigated by plotting real and imaginary parts of input impedance vs. frequency curve as shown in Fig. 4. From the plot of input impedance it can be observed that the real part of input impedance (resistance) has a value $50\ \Omega$, and imaginary part (reactance) has a very small

TABLE 2. Comparative analysis of gain, bandwidth and applications of the proposed antenna configurations.

Antenna Configuration	Strip Resonator	Resonant Frequency (GHz)	Bandwidth (-10 dB) GHz	Fractional Bandwidth (%)	Gain Variation (dBi)	Applications
Antenna 1	Only UWB antenna without strip resonator	3.6	3.2-3.9	19.71	0.9-6.7	Mid Band of 5G Applications
		7.5/10.9/13.5/16.4	5.7-17.5	101		UWB
Antenna 2	Antenna 1 & strip resonator 1	2.25	2.12-2.42	13.2	1.7-6.8	Bluetooth
		3.4	3.10-4.04	26.3		Mid Band of 5G Applications
		6.3/8.3/9.7/15/16.5	5.75-17.9	102		UWB
Antenna 3 (Proposed Antenna)	Antenna 1 & Strip resonator 1 & 2	2.1	1.96-2.21	12	1.4-6.4	WCDMA
		3.5	3.22-4.0	21.6		Mid Band of 5G Applications
		5.8/7.4/10.3/12/15.7	5.4-17.3	104		UWB

value nearly equal to zero. The resonant modes are at 2.1, 3.5, 5.8, 7.4, 10.3, 12, and 15.7 GHz, respectively.

Further, to validate the proposed antenna structure, an equivalent circuit model is developed by ADS simulator as shown in Fig. 5(a). The input port is excited through a 50 Ω RF connector. In the equivalent model, the microstrip feed inductance and static capacitance of antenna are represented by L_f and C_f , respectively. Inductance and capacitance due to circular patch are represented by parallel L_P-C_P . The parallel $L_{SP}-C_{SP}$ tuned cell represents the inductance and capacitance due to quad elliptical dumbbell shaped (QEDS) slotted patch, whose values depend upon the length of major-axis ‘a’ and minor-axis ‘b’ slots in the designed antenna. The coupling capacitor C_{in} at input represents the coupling between defected ground and slotted circular radiator. Further, the developed circuit model is simplified as shown in Fig. 5(b). The impedance of circular QEDS circular slotted patch is represented by series combination of Z_P and Z_{SP} . The impedance due to two meander line loaded strip resonators (MSRs) is represented by Z_{MSR} . The output port is terminated with 50 Ω load for impedance matching by input.

The impedance for quad elliptical dumbbell shaped slots can be expressed as [12, 33]:

$$Z_{slot} = j\omega \left(\sum_{k=1}^n L_k - \frac{1}{\omega^2} \sum_{k=1}^n \frac{1}{C_k} \right) \quad (1)$$

where $n(= 4)$ is the number of elliptical dumbbell shaped slots. The impedance for circular patch is given by [12, 33].

$$Z_p = \frac{1}{j\omega C_P} + j\omega L_p \quad (2)$$

The impedance due to circular patch and quad elliptical slots in patch can be written from Equations (1) & (2)

$$Z_{PATCH} = Z_{slot} + Z_p \quad (3)$$

The impedance of each parallel resonance circuit representing five frequencies is as given in Equations (4)–(8)

$$Z_1 = R_{g1} + j\omega L_{g1} + \frac{1}{j\omega C_{g1}} \quad (4)$$

$$Z_2 = R_{g2} + j\omega L_{g2} + \frac{1}{j\omega C_{g2}} \quad (5)$$

$$Z_3 = R_{g3} + j\omega L_{g3} + \frac{1}{j\omega C_{g3}} \quad (6)$$

$$Z_4 = R_{g4} + j\omega L_{g4} + \frac{1}{j\omega C_{g4}} \quad (7)$$

$$Z_5 = R_{g5} + j\omega L_{g5} + \frac{1}{j\omega C_{g5}} \quad (8)$$

The total impedance can be expressed as

$$Z_{UWB} = Z_1 + Z_2 + Z_3 + Z_4 + Z_5 \quad (9)$$

The impedance due to meander strip 1 and 2 resonators can be assumed as:

$$Z_{MSR1} = R_{s1} + j\omega L_{s1} + \frac{1}{j\omega C_{s1}} \quad (10)$$

$$Z_{MSR2} = R_{s2} + j\omega L_{s2} + \frac{1}{j\omega C_{s2}} \quad (11)$$

$$Z_{MSR} = Z_{MSR1} + Z_{MSR2} \quad (12)$$

Z_{UWB} and Z_{MSR} represent discontinuities present in ground plane while the total impedance is given by Z_{FREQ}

$$Z_{FREQ} = Z_{UWB} + Z_{MSR} + 50 \quad (13)$$

The impedance due to rectangle defected ground structure can be expressed as:

$$Z_{RDGS1} = j\omega L_{RDGS1} + \frac{1}{j\omega C_{RDGS1}} \quad (14)$$

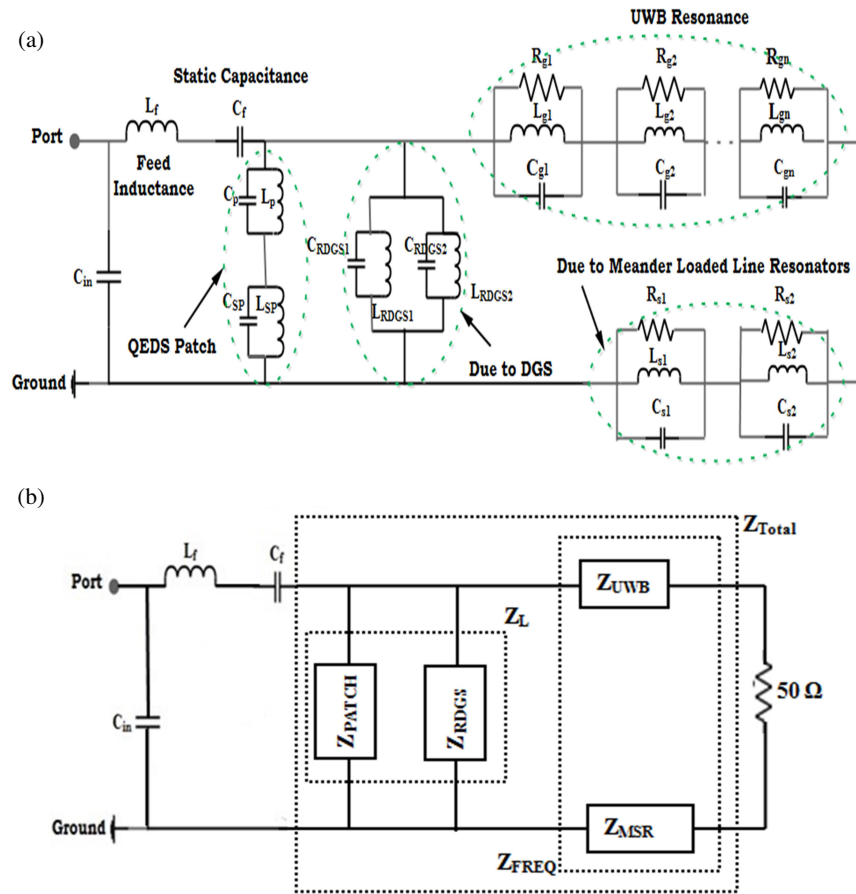


FIGURE 5. (a) Electrical equivalent model for DSQES antenna; (b) Simplified equivalent model.

$$Z_{RDGS2} = j\omega L_{RDGS2} + \frac{1}{j\omega C_{RDGS2}} \quad (15)$$

$$Z_{RDGS} = Z_{RDGS1} \parallel Z_{RDGS2} \quad (16)$$

Equivalent impedance of patch (Z_{PATCH}) and RDGS (Z_{RDGS}) from Equations (3) & (16) is given by Z_L

$$Z_L = \frac{(Z_{PATCH}) \cdot (Z_{RDGS})}{(Z_{PATCH}) + (Z_{RDGS})} \quad (17)$$

The total impedance from Equations (13) & (17) is given by

$$Z_{Total} = \frac{(Z_L) \cdot (Z_{FREQ})}{(Z_L) + (Z_{FREQ})} \quad (18)$$

The impedance of feed is given by

$$Z_{feed} = \frac{1}{j\omega C_f} \quad (19)$$

The total impedance from Equations (18) & (19) is given by

$$Z_T = \left(Z_{Total} + \frac{1}{j\omega C_f} \right) \quad (20)$$

Therefore, the impedance of the whole equivalent circuit is given by

$$Z_{Eq} = j\omega L_f + \frac{(Z_T) \cdot \frac{1}{(j\omega C_{in})}}{(Z_T) + \frac{1}{(j\omega C_{in})}} \quad (21)$$

Input reflection coefficient of the circuit is given by

$$S_{11} = \frac{(Z_{Eq}) - 50}{(Z_{Eq}) + 50} \quad (22)$$

2.2. Design Method of the Proposed Antenna

The proposed antenna is designed in following steps:

Step 1: In the first step, radius R of circular patch is calculated with the help of Equations (23) and (24) for the confirmation of estimated lowest resonant frequency as given by [37].

$$R = \frac{92 \times 10^9}{fr \sqrt{(\epsilon_{eff})}} \quad (23)$$

$$\epsilon_{eff} = \frac{(\epsilon_r + 1)}{2} \quad (24)$$

Step 2: Four elliptical shaped slots are inserted in the circular patch, and major and minor axes of ellipse are calculated by

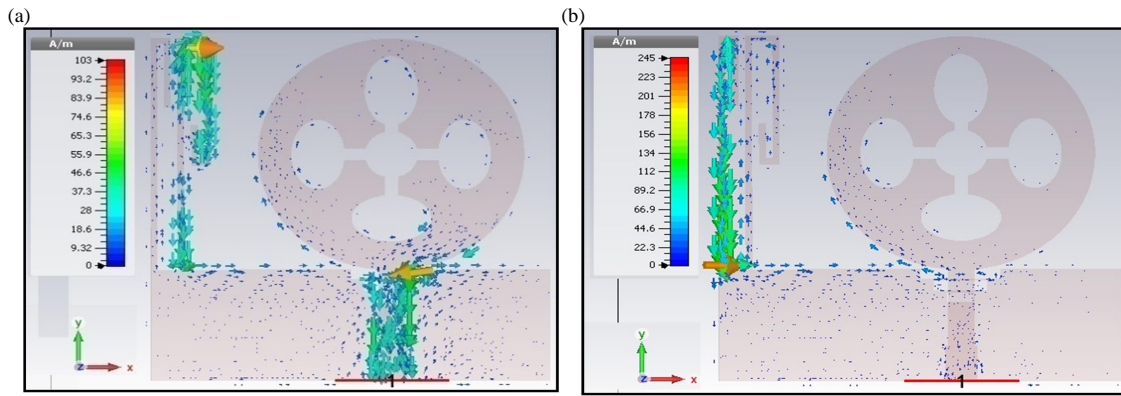


FIGURE 6. Surface current distribution plot of the proposed antenna at different resonating frequencies (a) 2.1 GHz, (b) 3.5 GHz.

Equation (25)

$$\frac{x^2}{a^2} + \frac{y^2}{b^2} = 1 \quad (25)$$

where ‘ a ’ and ‘ b ’ are the lengths of major axis and minor axis besides x and y directions, and optimized value $a = 6$ mm and $b = 4$ mm.

Step 3: In the third step, the length of meander strip resonator is calculated by the help of Equation (26), and the length of the n th $\lambda_g/4$ meander strip resonator is calculated from corresponding resonant frequency (f_{rn}). The total length $L_{y_{sn}}$ of meander strip resonator depends on two factors, resonant frequency f_{rn} and effective dielectric constant ϵ_{eff} of the substrate as given by [36].

$$L_{y_{sn}} = \frac{c}{4f_{rn}\sqrt{(\epsilon_{eff})}} \quad n = 1, 2, 3, \dots \quad (26)$$

where λ_g and c are the guided wavelength and speed of light, respectively. $L_{y_{sn}}$ denotes the total length of the n th meander strip resonator, and resonating frequency depends upon $L_{y_{sn}}$.

In step 1, a patch antenna of circular shape is designed by keeping lower value of resonant frequency (f_r) as 5.8 GHz. The approximate values of patch radius R , obtained from calculation and simulation, are 9.8 mm and 10 mm, respectively, which are very close to each other. It can be observed that the first resonance is obtained at 2.1 GHz with MSR-2 as reflected through surface current plot shown in Figs. 6(a) and 6(b). It can also be observed that the current length is equal to quarter of the guided wavelength (λ_g). To calculate the total length of MSR-2 the formula as given in Equation (27) is used.

$$L_{y_{s2}} = L_4 + L_5 + L_6 + L_7 + L_8 \approx \lambda_g/4 \quad (27)$$

Using the parameters as given in Table 1, the length of MSR-2 ($L_{y_{s2}}$) is 38 mm. From Equation (24), the value of ϵ_{eff} is 2.65. The value of the first resonant frequency f_{r1} obtained from calculation is 1.81 GHz, and from simulation it is 2.1 GHz which are approximately equal. Further, MSR-1 is accountable for the second resonant frequency f_{r2} , and its length can be calculated by the help of Equation (28)

$$L_{y_{s1}} = L_1 + L_2 + L_3 \approx \lambda_g/4 \quad (28)$$

As given in Table 1, $L_{y_{s1}} = 27.5$ mm. Hence, the calculated value of second resonant frequency is $f_{r2} = 2.72$ GHz. However, the value of the 2nd resonant frequency obtained after simulation is 3.5 GHz, which is very close to designed value. Therefore, the procedure used in designing the proposed antenna structure is also validated by applying full-wave simulation method. The proposed antenna configuration of antenna is matched to the theoretical prospective.

2.3. Parametric Analysis

To realize the effect of resonance parameters on the performance of antenna, a parametric investigation is carried out. The effect of circular patch radius R , inner radius r , length of major axis ‘ a ’, length of minor axis ‘ b ’ of elliptical slots, length $L_{y_{s1}}$ of MSR-1 and $L_{y_{s2}}$ of MSR-2 are sufficient for the optimization of antenna impedance characteristics which can be observed from Fig. 7. The variation of radius R affects first resonating band and UWB band. Fig. 7(a) shows the effect of variation of radius R on return loss. On varying the value of R from 9 mm to 11 mm, a shift of 0.1 GHz towards lower side is observed in f_{r1} , whereas 0.1 GHz shift in advance side is observed in higher cutoff frequency. The optimized value of R is obtained as 10 mm, which covers all required operating frequencies. The variation of inner radius r mostly affects the first and last resonating frequencies of UWB as shown in Fig. 7(b). As r is varied from 1 mm to 3 mm the first resonating frequency of UWB is shifted to higher side, and an optimized value of $r = 2$ mm is chosen to achieve the desired result. In the next step, the variation of major axis length ‘ a ’ and minor axis length ‘ b ’ has been done. The major axis length ‘ a ’ is varied from 5 to 7 mm and minor axis length ‘ b ’ from 3 to 5 mm. A small shift in resonating frequency can be observed due to this variation, and an optimized value of ‘ a ’ = 6 mm and ‘ b ’ = 4 mm is selected for the proposed antenna effect of variation as shown in Fig. 7(c). Further, Fig. 7(d) shows the effect of variation of length of MSR-1. It is clear from the figure that when $L_{y_{s1}}$ changes from 26.5 to 28.5 mm, other parameters are stable, and due to this variation, the second resonating frequency f_{r2} changes from 3.48 to 3.52 GHz while the first resonating frequency and UWB remain unchanged as shown in

TABLE 3. Variation of the second resonant frequency f_{r2} with the length of MSR-1.

L_3 (mm)	L_{ys1} (mm)	f_{r2} (GHz)	
		Design Equation (6)	Simulated Value
5	26.5	2.83	3.48
6	27.5	2.72	3.50
7	28.5	2.63	3.52

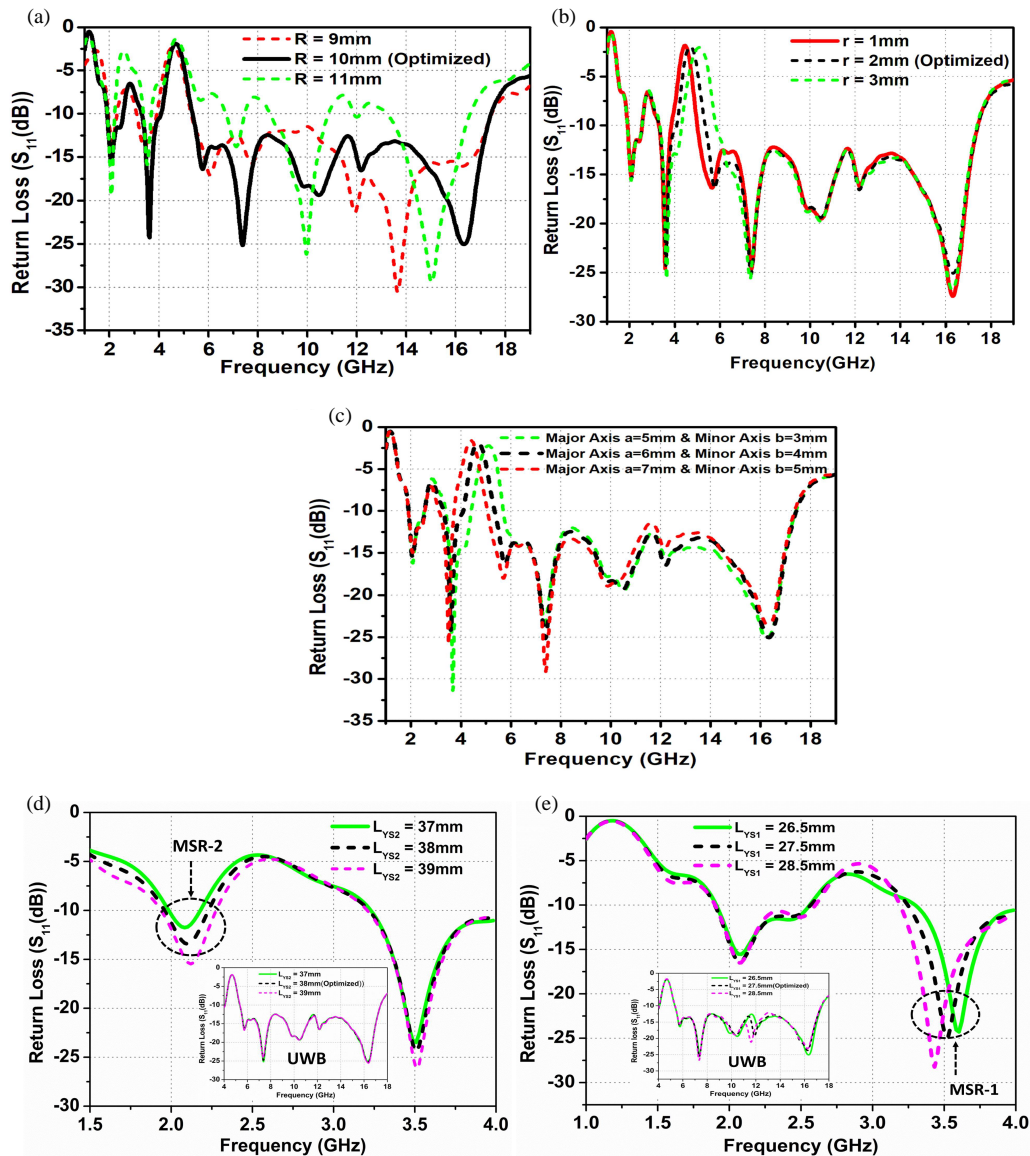


FIGURE 7. Return loss (dB) variation of proposed antenna (a) when radius R changes; (b) when inner radius r changes; (c) major axis length ‘ a ’ and minor axis length ‘ b ’ changes; (d) meander strip length L_{ys2} changes; (e) meander strip length L_{ys1} changes.

Fig. 7(d). The optimized length of $L_{ys1} = 27.5$ mm is preferred to cover mid-band of 5G applications. In Table 3, different values of the second resonant frequency f_{r2} with variation in L_{ys1} are given from simulated and calculated results. It can be observed that the calculated values of frequency f_{r2} are in accordance with simulated ones.

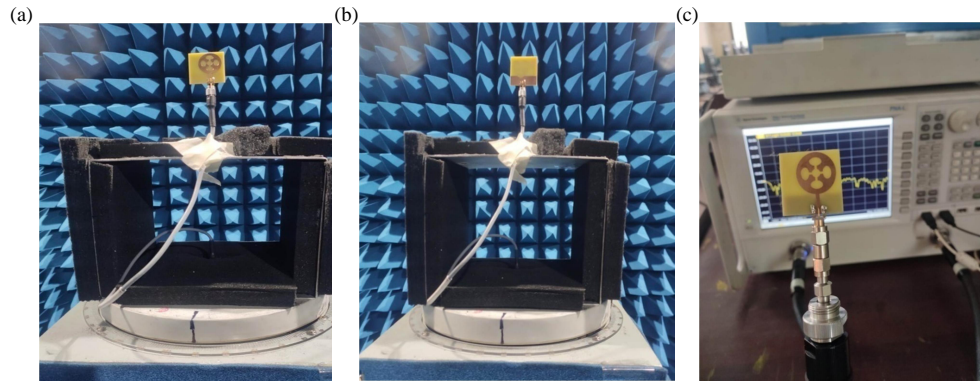
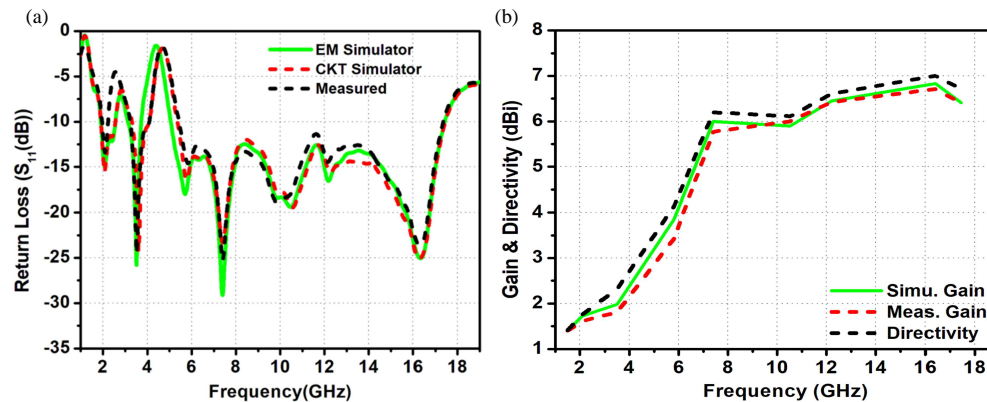
Further, the effect of variation of the length of MSR-2 is as given in Fig. 7(e). By keeping other parameters fixed when length L_{ys2} is varied from 37 mm to 39 mm, the first resonat-

ing frequency f_{r1} changes from 2.12 GHz to 2.08 GHz while the second resonating frequency and UWB of antenna remain unchanged. It can be observed that the variation in f_{r1} along with UWB depends upon length L_{ys2} .

In order to operate in WCDMA band, optimized length $L_{ys2} = 38$ mm is chosen. From Table 4 it can be observed that the first resonant frequency f_{r1} varies with L_{ys2} . Further, it can also be observed that the simulated value of f_{r1} is in accordance with calculated value.

TABLE 4. Variation of the first resonant frequency f_{r1} with the length of MSR-2.

L_8 (mm)	L_{ys2} (mm)	f_{r1} (GHz)	
		Design Equation (5)	Simulated Value
2	37	2	2.12
3	38	1.81	2.10
4	39	2.70	2.08

**FIGURE 8.** Measurement setup for proposed antenna. (a) Antenna front view. (b) Antenna backview. (c) $|S_{11}|$ measurement.**FIGURE 9.** (a) Simulated and measured return loss (S_{11}) dB plot for proposed antenna. (b) Simulated and measured gain vs. frequency plot.

It can be concluded from parametric variation that separate tuning of meander strip resonators does not affect UWB characteristics and has independent resonating frequency.

3. RESULTS AND DISCUSSIONS

The fabrication of the proposed antenna structure has been done on an FR-4 substrate with the help of caddo-71 prototype machine. The return loss was measured by using an ENA series vector network analyzer (VNA) with the setup as shown in Fig. 8.

The variation of measured and simulated return losses of fabricated and designed antenna is shown in Fig. 9(a). A good agreement has been observed between simulated and measured results. Slight variations can occur due to some constraint during fabrication, uncertainties present in dielectric material, different substrate thicknesses and effects due to soldering. The proposed designed antenna resonates at 2.1, 3.5, 5.8, 7.4, 10.3,

12, 15.7 GHz frequencies. It also covers two separate lower frequency communication bands 2100 MHz (1.96–2.21 GHz) and 3500 MHz (3.22–4 GHz) along with UWB (5.4–17.3 GHz), and the respective fractional bandwidths are 12, 21.6, and 104%. Further, the measured gain and directivity of proposed antenna are obtained through broadband horn antenna (as reference antenna). Furthermore, the measured gain/directivity versus frequency variation is shown in Fig. 9(b). The directivity of antenna is varied between 1.4 and 7 dBi in the entire frequency band of 1.96–17.3 GHz. It can be observed that the maximum directivity is obtained at 15.7 GHz resonating frequency. Furthermore, the gains for MSR-1 band, MSR-2 band, and UWB have been measured and found to be 1.40–1.72 dBi, 1.8–2.3 dBi, and 3–6.4 dBi, respectively. It is also found that the gain discrepancy is less than ± 0.5 dBi. The measured peak gains are obtained and compared with previously reported antennas as mentioned in Table 5.

TABLE 5. Conductivity and dielectric property of breast model.

Material	Conductivity (σ) (S/m)	Relative Permittivity (ϵ_r)
Skin	1.1	37
Tumour	4	50

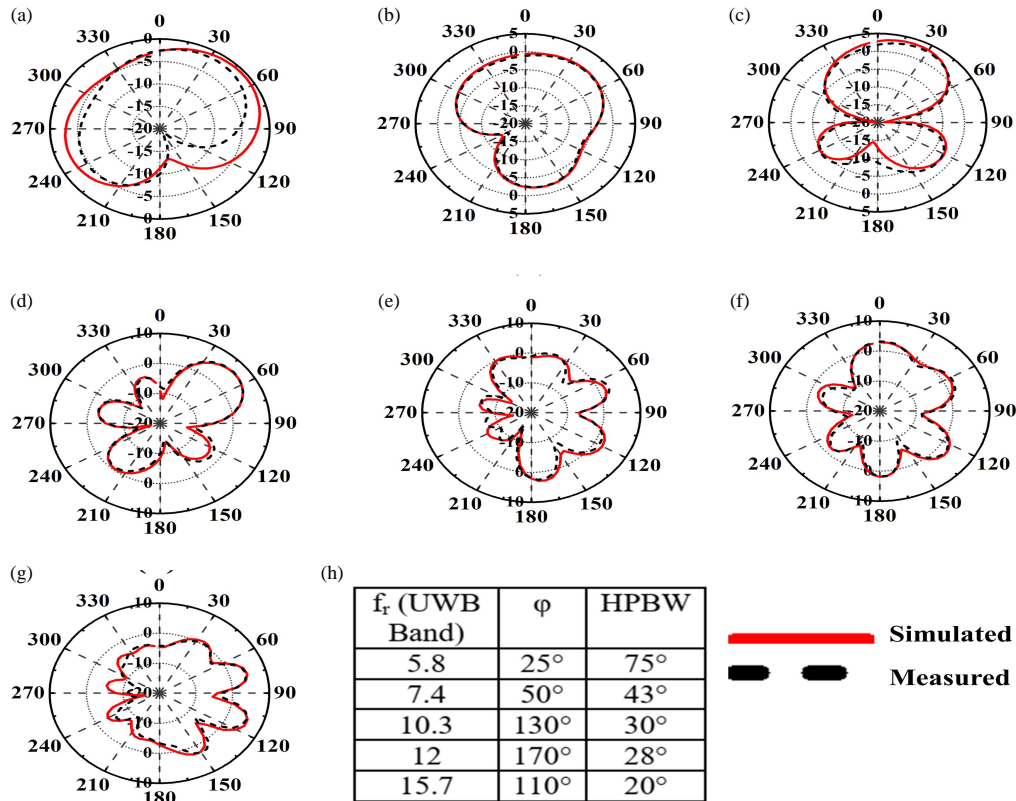


FIGURE 10. Simulated and measured radiation pattern of the proposed antenna configuration at different resonating frequencies: (a) 2.1 GHz, (b) 3.5 GHz, (c) 5.8 GHz, (d) 7.4 GHz, (e) 10.3 GHz, (f) 12 GHz, (g) 15.7 GHz, and $\theta = 90^\circ$ in x - y plane, (h) HPBW variation with ϕ .

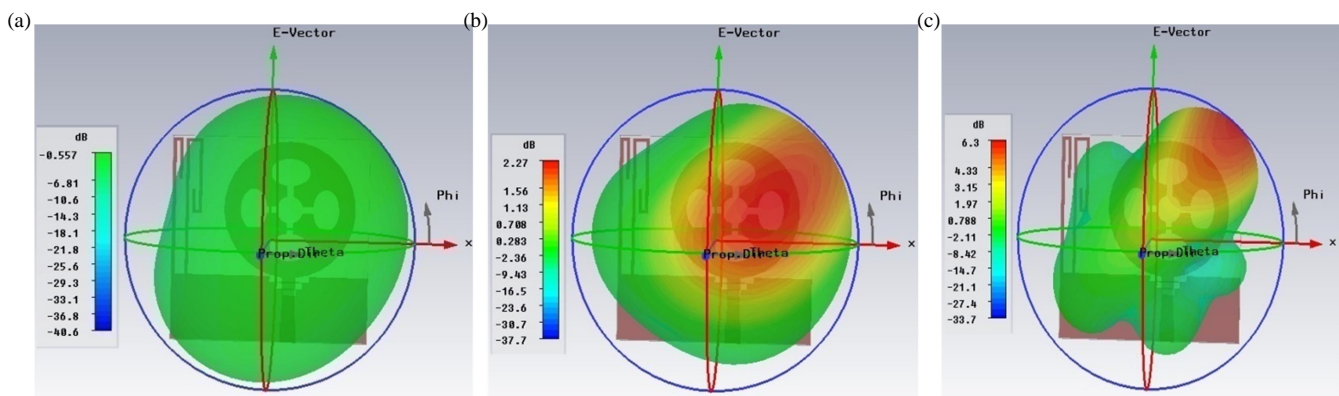


FIGURE 11. 3D simulated radiation pattern of proposed antenna: (a) 2.1 GHz, (b) 3.5 GHz, (c) 7.4 GHz, respectively.

The simulated and measured radiation patterns of the proposed antenna are shown in Fig. 10 for different resonating frequencies 2.1, 3.5, 5.8, 7.4, 12, and 15.7 GHz at $\theta = 90^\circ$ and x - y plane. It can be observed from Fig. 10 that a good agreement

is obtained between simulated and measured radiation patterns with minor disparity. The designed antenna gives an omnidirectional radiation pattern at lower resonant frequencies of 2.1 and 3.5 GHz. However, almost directional characteristics

TABLE 6. Comparative performance analysis of the proposed antenna with previously reported antennas.

Reported Antennas	Antenna Size, [mm ²]	Antenna Response	Operating BW (GHz)	Fractional BW (%)	Peak Gain (dBi)	HPBW moves between (°)	Application for operating band
[10]	30×30	Single Band	4-18	127	9.3	52°-30°	UWB
[11]	50×50	Single Band	3.4-10	98	NA	47°-30°	UWB
[12]	50×50	Single Band	4.1-11.5	95	8.4	49°-22°	UWB
[13]	32×32	Single Band	9.7-14.5	39	10.7	35°-26°	Wideband
[14]	42×50	Single Band	2.4-10.4	125	6.5	105°-50°	UWB
[15]	40×40	Single Band	4.4-10.6	82	9.1	44°-29°	UWB
[17]	24×30	Triple Band	2.43-2.67	9	1.75	NA	Wi-Max
			3.37-3.58	6	1.9	NA	Wi-Max
			5.1-5.65	10	1.9	NA	WLAN
[21]	12×20	Dual Band	2.4-2.52	2	1.6	NA	WLAN
			3.2-10.6	107	4	NA	UWB
[22]	35×24	Dual Band	2.4-2.48	3	1.8	NA	Bluetooth
			3.1-10.6	109	3.8	NA	UWB
[23]	40×40	Multi Band	4.93-5.8	16	1.5	NA	Wi-Max
			5.9-6.7	13	2.4	NA	C-Band
			9.28-10.2	9	4	NA	X-Band
			3.0-12	120	5	NA	UWB
[24]	50×65	Dual Band	1.92-2.17	12	NA	NA	UMTS
			3.0-11.0	114	NA	NA	UWB
[26]	23×23	Single band	3.20-5.34	50	2.76	NA	5G devices
[27]	60×50	Triple Band	2.05-3.05	39	1.5	NA	Bluetooth
			3.65-3.92	7	2.8	NA	WLAN
			5.24-10.75	68	8.03	NA	UWB
[29]	12×14	Triple Band	6.22-6.44	3.46	3.07	NA	C
			8.92-9.05	1.44	4.78	NA	X
			12.92-13.20	2.14	7.73	NA	Ku
[30]	30×30	Quad Band	1.56-1.62	3.7	-0.8	NA	GPS
			2.30-2.51	8.7	1.0	NA	WLAN
			3.40-3.77	10	1.7	NA	Wi-Max
			5.05-6.15	19	3.7	NA	Sub-6 GHz
[31]	80×80	Quad Band	1.55-1.59	2.5	3.49	NA	GPS
			2.43-2.52	3.6	6.49	NA	IRNSS
			3.44-3.54	2.8	4.93	NA	Sub-6 GHz
			5.23-5.32	1.7	4.46	NA	WLAN
[36]	30×30	Multi Band	2-2.2	9	1.6	NA	WCDMA
			2.34-2.47	6	2.7	NA	Bluetooth
			2.69-2.75	3	2.4	NA	Wi-Max
			4-18	127	4.4	NA	UWB
Proposed Antenna	30 × 30	Multi-band	1.96-2.21	12	1.73	117°	WCDMA
			3.22-4.0	21.6	2.3	147°	Mid-band of 5G applications
			5.4-17.3	104	6.4	20°-75°	UWB

are obtained at resonant frequencies of 5.8, 7.4, 10.3, 12, and 15.7 GHz in the UWB of 5.4–17.3 GHz. Further, half power beamwidth (HPBW) moves from x -axis $\Phi = 25^\circ$ to $\Phi = 170^\circ$ in x - y plane. Therefore, least HPBW from 75° to 20° degrees

is obtained as compared with previous reported antennas [10–15, 17, 21–24, 26, 27, 29–31, 36].

The corresponding 3-D radiation patterns are shown in Fig. 11. It is observed that the omnidirectional radiation

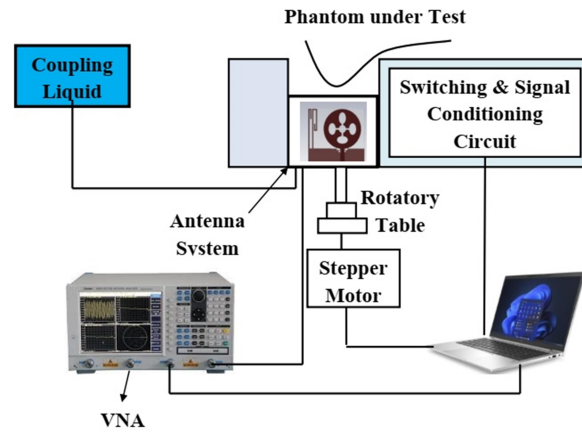


FIGURE 12. UWB-MI setup for microwave tumour detection.

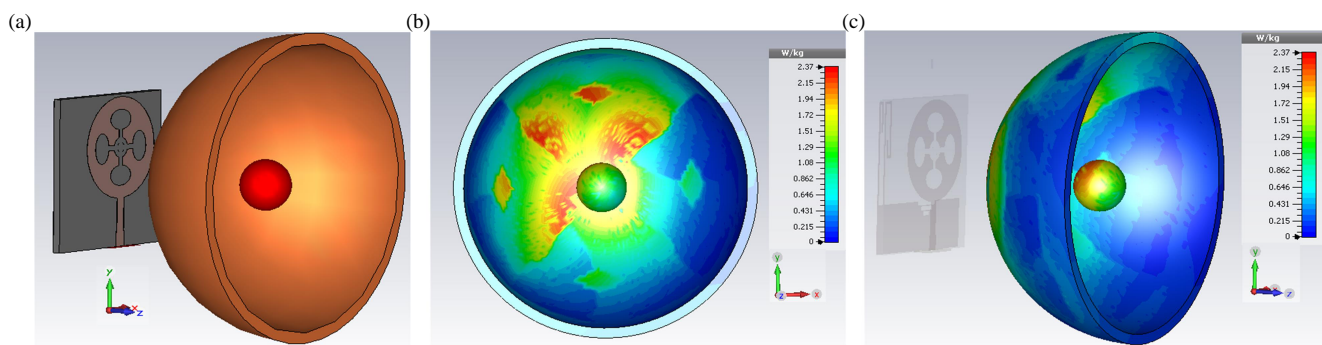


FIGURE 13. Experimental setup: (a) Breast model and antenna, (b) front view of simulated SAR distribution, (c) side view of simulated SAR distribution.

patterns are obtained for 2.1 GHz and 3.5 GHz frequency; it is also analogous with Figs. 10(a), 10(b). Therefore, the maximum radiation intensity in particular directions can be observed at 3.5 GHz and 7.4 GHz resonant frequencies, and it is established by Figs. 11(b) and 11(c), respectively.

4. APPLICATION OF PROPOSED ANTENNA IN MICROWAVE TUMOUR DETECTION

In current scenario, UWB-MI is widely used because of non-ionizing signals used as compared to traditional mammography techniques. It works on the principle of distinguishing dielectric properties of normal breast/tumour cell. The dielectric properties of tumour cells are higher than normal breast tissue as tumour cell scatters higher microwave signals [34]. Using UWB-MI technique, microwave pulses are transmitted by antenna towards targeted object, and scattered pulses are received from different directions. As can be seen in Fig. 12, UWB antenna is connected to vector network analyser (VNA) [35]. An antenna system can be used to get scattered signal and process through switching and signal conditioning circuit. Therefore, antenna can be used as a sensor, and through coupling liquid the penetration of signal can be increased. Hence, the proposed directional UWB antenna can be used to detect high resolution image and deep penetration into natural tissues.

Experimental setup for proposed antenna is shown in Fig. 13. In the proposed setup, a breast model is designed with dielectric properties as given in Table 5, where σ is the conductivity, and ϵ_r is the relative permittivity as given by [38]. The model consists of a hemisphere of 50 mm radius in 2 mm layer of skin tissue. A spherical tumour of 5 mm radius is used for analysis. The centre of antenna is placed at origin, and the distance between breast model and antenna is 10 mm. Figs. 13(b) and 13(c) show the simulated Specific Absorption Rate (SAR) distribution on breast model. From the simulation results, it can be observed that a significant amount of energy is absorbed by tumour, but little power is deposited in skin tissue due to its low conductivity.

5. CONCLUSIONS

In the proposed work, a dumbbell shape quad elliptical slotted directional UWB antenna integrated with meander strip resonators strips is designed, fabricated, and tested experimentally. To recognize multiband characteristics, two meander-strip-resonators are loaded on ground plane for WCDMA and mid-band of 5G applications without troubling directional UWB features. The measured impedance bandwidth of designed UWB antenna is 5.4–17.3 GHz with 104% FBW with two additional lower bands 1.96–2.21 GHz and 3.22–4.07 GHz. The designed antenna operates into

seven resonant modes of 2.1/3.5/5.8/7.4/10.3/12/15.4 GHz by adding/inserting slotted structure approach. Also, mathematical validation of designed antenna is carried out with electrical equivalent circuit to discuss directional UWB phenomenon using ADS simulator. Further, HPBW and gain of designed antenna are attained between 70° – 20° and 1.7–6.4 dBi, respectively. The main lobes of designed antenna are more directional with high gain characteristics. Hence, it is suitable for microwave tumour detection as demonstrated. Furthermore, antenna size, FBW, HPBW, and gain characteristics of designed antenna are compared with reported literature as given in Table 6.

ACKNOWLEDGEMENT

The Authors would like to concede and express their earnest thanks to Rajasthan Technical University (RTU) Kota for providing the measurement lab facilities during this research work.

REFERENCES

- [1] Desai, A., T. K. Upadhyaya, R. Patel, S. Bhatt, and P. Mankodi, "Wideband high gain fractal antenna for wireless applications," *Progress In Electromagnetics Research Letters*, Vol. 74, 125–130, 2018.
- [2] Chen, Z. N., T. S. P. See, and X. Qing, "Small printed ultrawideband antenna with reduced ground plane effect," *IEEE Transactions on Antennas and Propagation*, Vol. 55, No. 2, 383–388, 2007.
- [3] Radiom, S., H. Aliakbarian, G. A. E. Vandenbosch, and G. G. E. Gielen, "An effective technique for symmetric planar monopole antenna miniaturization," *IEEE Transactions on Antennas and Propagation*, Vol. 57, No. 10, 2989–2996, Oct. 2009.
- [4] Gopikrishna, M., D. D. Krishna, C. K. Anandan, P. Mohanan, and K. Vasudevan, "Design of a compact semi-elliptical monopole slot antenna for UWB systems," *IEEE Transactions on Antennas and Propagation*, Vol. 57, No. 6, 1834–1837, Jun. 2009.
- [5] Abbosh, A. M. and M. E. Bialkowski, "Design of ultrawideband planar monopole antennas of circular and elliptical shape," *IEEE Transactions on Antennas and Propagation*, Vol. 56, No. 1, 17–23, 2008.
- [6] Sagar, N. T., M. L. Meena, and P. Shukla, "Design and performance analysis of UWB circular ring antenna with defected ground structure," *ICTACT International Journal on Communication Technology*, Vol. 8, No. 4, 1656–1663, 2017.
- [7] Li, G., H. Zhai, T. Li, X. Y. Ma, and C.-H. Liang, "Design of a compact UWB antenna integrated with GSM/WCDMA/WLAN bands," *Progress In Electromagnetics Research*, Vol. 136, 409–419, 2013.
- [8] Gaber, M., F. Fouad, A. Yahia, M. El-Aasser, and N. Gad, "A printed antenna design with defected ground structure for multi-band applications," *European Journal of Science and Technology*, No. 28, 1528–1533, 2021.
- [9] Meena, M. L., M. Kumar, and G. Parmar, "Modified unidirectional circular patch antenna with parabolic shape ground plane having T-slots for microwave links," *ICTACT International Journal on Communication Technology*, Vol. 6, No. 2, 1087–1090, 2015.
- [10] Gupta, A. and M. L. Meena, "Design of semi circular floral shape directive UWB antenna for radar based microwave imaging," in *2021 International Conference on Artificial Intelligence and Smart Systems (ICAIS)*, 1188–1192, Coimbatore, India, 2021.
- [11] Meena, M. L., G. Parmar, and M. Kumar, "Parabolic shape ground plane having T-slots directional UWB antenna for airborne radar system," in *2015 International Conference on Computer, Communication and Control*, 1–3, Indore, India, 2015.
- [12] Meena, M. L., M. Kumar, G. Parmar, and R. S. Meena, "Design analysis and modeling of directional UWB antenna with elliptical slotted ground structure for applications in C- & X-bands," *Progress In Electromagnetics Research C*, Vol. 63, 193–207, 2016.
- [13] Meena, M. L., M. Kumar, G. Parmar, and R. S. Meena, "Design and analysis of directional wideband circular ring antenna with square slotted ground structure for radar systems," *International Journal of Microwave and Optical Technology*, Vol. 12, No. 1, 59–68, 2017.
- [14] Sagar, N. T., M. L. Meena, and P. Shukla, "Design and performance analysis of UWB circular ring antenna with defected ground structure," *ICTACT International Journal on Communication Technology*, Vol. 8, No. 4, 1656–1663, 2017.
- [15] Meena, M. L. and M. Kumar, "Design of high gain/directional ultra-wideband antenna for radar imaging systems," *International Journal of RF and Microwave Computer-Aided Engineering*, Vol. 29, No. 2, e21543, Feb. 2019.
- [16] Roy, S., J.-J. Tiang, M. B. Roslee, M. T. Ahmed, and M. A. Parvez, "The frequency-independent wideband planar log-periodic antenna for multiband applications," *Turkish Journal of Computer and Mathematics Education*, Vol. 12, No. 8, 2037–2043, 2021.
- [17] Galav, K. and M. L. Meena, "Design and analysis of compact printed triple band antenna for Wi-MAX, WLAN and wireless systems," *ICTACT Journal on Microelectronics*, Vol. 6, No. 1, 866–871, 2020.
- [18] Singh, P. P. and S. K. Sharma, "Design and fabrication of a triple band microstrip antenna for WLAN, satellite TV and radar applications," *Progress In Electromagnetics Research C*, Vol. 117, 277–289, 2022.
- [19] Sun, X.-B., "Design of a triple-band antenna based on its current distribution," *Progress In Electromagnetics Research Letters*, Vol. 90, 113–119, 2020.
- [20] Galav, K. and M. L. Meena, "Design and analysis of quad band antenna for wireless systems," *ICTACT Journal on Microelectronics*, Vol. 5, 866–871, 2020.
- [21] Naidu, P. V., "Design, simulation of a compact triangular shaped dual-band microstrip antenna for 2.4 GHz Bluetooth/WLAN and UWB applications," *Wireless Personal Communications*, Vol. 95, No. 2, 783–794, 2017.
- [22] Mahamine, S. D., R. S. Parbat, S. H. Bodake, and M. P. Aher, "Design of Bluetooth integrated UWB printed monopole antenna for wireless application," in *2016 International Conference on Automatic Control and Dynamic Optimization Techniques (ICACDOT)*, 1146–1151, 2016.
- [23] Pahadsingh, S. and S. Sahu, "Planar UWB integrated with multi narrowband cylindrical dielectric resonator antenna for cognitive radio application," *AEU-International Journal of Electronics and Communications*, Vol. 74, 150–157, 2017.
- [24] Aravind, S., S. Joseph, S. Mridula, B. Paul, and P. Mohanan, "Compact dual band antenna for GSM1800/1900/UMTS/LTE/UWB," *Procedia Computer Science*, Vol. 46, 1349–1356, 2015.
- [25] Daghari, M., C. Essid, and H. Sakli, "Multi-UWB antenna system design for 5G wireless applications with diversity," *Wireless Communications and Mobile Computing*, Vol. 2021, Article ID 9966581, 2021.
- [26] Kapoor, A., R. Mishra, and P. Kumar, "Wideband miniaturized patch radiator for sub-6 GHz 5G devices," *Heliyon*, Vol. 7, No. 9,

- e07931, 2021.
- [27] Srivastava, K., A. Kumar, B. K. Kanaujia, S. Dwari, and S. Kumar, "Multiband integrated wideband antenna for Bluetooth/WLAN applications," *AEU-International Journal of Electronics and Communications*, Vol. 89, 77–84, 2018.
- [28] Sohi, A. K. and A. Kaur, "Computational analysis of a dual-port semi-circular patch antenna combined with Koch curve fractals for ultra-wideband systems," *Engineering Reports*, Vol. 3, No. 9, e12378, 2021.
- [29] Suvarna, K., N. Ramamurthy, and D. V. Vardhan, "A tri-band miniaturized antenna using fractal defected ground structure for C/X and Ku-band applications," *Progress In Electromagnetics Research M*, Vol. 113, 115–128, 2022.
- [30] Ren, W. and P. Yang, "A tri-mode hybrid antenna for quad-band applications," *Progress In Electromagnetics Research Letters*, Vol. 111, 45–54, 2023.
- [31] Patel, D. H. and G. D. Makwana, "Multiband antenna for GPS, IRNSS, sub-6 GHz 5G and WLAN applications," *Progress In Electromagnetics Research M*, Vol. 116, 53–63, 2023.
- [32] Kumari, S., Y. K. Awasthi, and D. Bansal, "A miniaturized circularly polarized multiband antenna for Wi-MAX, C-band & X-band applications," *Progress In Electromagnetics Research C*, Vol. 125, 117–131, 2022.
- [33] Majumdar, A., S. K. Das, and A. Das, "Ultra wide band CPW fed patch antenna with fractal elements and DGS for wireless applications," *Progress In Electromagnetics Research C*, Vol. 94, 131–144, 2019.
- [34] Conceição, R. C., J. J. Mohr, and M. O'Halloran, *An Introduction to Microwave Imaging for Breast Cancer Detection*, Springer, 2016.
- [35] Mahmud, M. Z., M. T. Islam, N. Misran, A. F. Almutairi, and M. Cho, "Ultra-wideband (UWB) antenna sensor based microwave breast imaging: A review," *Sensors*, Vol. 18, No. 9, 2951, 2018.
- [36] Meena, M. L. and A. Gupta, "Design analysis of a semi-circular floral shaped directional UWB antenna integrated with wireless multiband applications," *Progress In Electromagnetics Research C*, Vol. 90, 155–167, 2019.
- [37] Balanis, C. A., *Antenna Theory: Analysis and Design*, 3rd ed., John Wiley & Sons, 2016.
- [38] Amdaouch, I., O. Aghzout, A. Naghar, A. V. Alejos, and F. J. Falcone, "Breast tumor detection system based on a compact UWB antenna design," *Progress In Electromagnetics Research M*, Vol. 64, 123–133, 2018.